Thickness of pyroclastic cover beds: the case study of Mount Albino (Campania region, southern Italy)

Fabio Matano, Giovanna De Chiara, Settimio Ferlisi & Leonardo Cascini

Taylor & Francis
Taylor & Francis Group

SCIENCE

Thickness of pyroclastic cover beds: the case study of Mount Albino (Campania region, southern Italy)

Fabio Matano[a] , Giovanna De Chiara[b] , Settimio Ferlisi[b] and Leonardo Cascini[b]

[a]Istituto per l'Ambiente Marino Costiero (IAMC), Consiglio Nazionale delle Ricerche (CNR), Napoli, Italy; [b]Department of Civil Engineering, University of Salerno, Fisciano, SA, Italy

ABSTRACT

The paper presents a method for estimating and mapping – at detailed scale (1:5000) – the thickness of pyroclastic cover beds resting on calcareous bedrock. This method, tested in the study area of Mount Albino (Campania region, southern Italy), makes use mainly of information gathered from *in situ* investigations, managed and processed in a geographical information system environment via a geostatistical interpolation technique (i.e. ordinary kriging) and finally integrated and amended by adopting a heuristic approach. Given its easy applicability and affordable costs, the proposed method can be used in similar geological contexts where knowledge of the spatial distribution of pyroclastic cover beds is a requirement for understanding and predicting slope instability processes.

1. Introduction

In the Campania region (southern Italy), where a number of moderate to steep slopes are near active volcanic centres (Figure 1(a)), surface materials consist mainly of pyroclastic cover beds. These pyroclastic air-fall deposits are locally characterised by very complex stratigraphy, in turn reflecting a marked heterogeneity of both the physical and mechanical properties of the different constituent lithotypes. Actual values of the pyroclastic cover bed thickness (i.e. the depth of its lithological contact with the underlying bedrock from the topographic surface) are largely controlled by explosive volcanism intensity, buried morphology of the top of bedrock and erosion and transport processes (transport-limited slopes according to Taylor & Eggleton, 2001). Moreover, the variability of thickness in space and time is a result of the combined influence primarily of air-fall tephra distribution axes, climate and relief (elevation, slope orientation and incline) and secondarily of vegetation and land use.

The thickness of pyroclastic cover beds controls surface and subsurface processes; it affects runoff generation, erosion, subsurface and groundwater flow, mass movement and, consequently, landscape evolution (Amundson, Heimsath, Owen, Yoo, & Dietrich, 2015; Catani, Segoni, & Falorni, 2010; Dietrich, Reiss, Hsu, & Montgomery, 1995; Kuriakose, Devkota, Rossiter, & Jetten, 2009; Lucà, Buttafuoco, Robustelli, & Malafronte, 2014). Therefore quantitative estimation of the spatial distribution of pyroclastic cover bed thickness should be regularly included among the activities required to carry out susceptibility and

hazard analyses of slope instabilities on natural slopes (De Chiara, Ferlisi, Cascini, & Matano, 2015; Segoni, Rossi, & Catani, 2012; Uchida, Tamura, & Akiyama, 2011).

Using the Mount Albino area in the municipal territory of Nocera Inferiore (near Salerno city, Italy) as an example, this paper aims to provide an integrated procedure for estimating and mapping at a detailed scale (1:5000) the thickness of pyroclastic cover beds resting on calcareous bedrock. The proposed method relies on input data collected via a low-cost but very intensive and rigorous field sampling campaign (based on probings, dynamic penetration tests, geophysical surveys and hand-dug pits) and supplemented by information gathered from geological field surveys, air-photo interpretation and digital terrain model (DTM) analysis. Its repeatability is a result of a proper use of geostatistical techniques for interpolation of thickness data (i.e. ordinary kriging (O.K.)) combined with manual adjustments in a geographical information system (GIS) environment.

2. The study area

The northern slope of Mount Albino is about 400 ha in area and encompasses 10 mountain catchments (Figure 1(b)). It is located in the geological context labelled A1 by Cascini, Ferlisi, and Vitolo (2008) (Figure 1(a)) where late Pleistocene-Holocene pyroclastic cover beds, deriving from the explosive activity of Somma-Vesuvius and Phlegraean Fields volcanic complexes (De Vita, Napolitano, Godt, & Baum, 2012; Rolandi, Paone, Di Lascio, & Stefani, 2007),
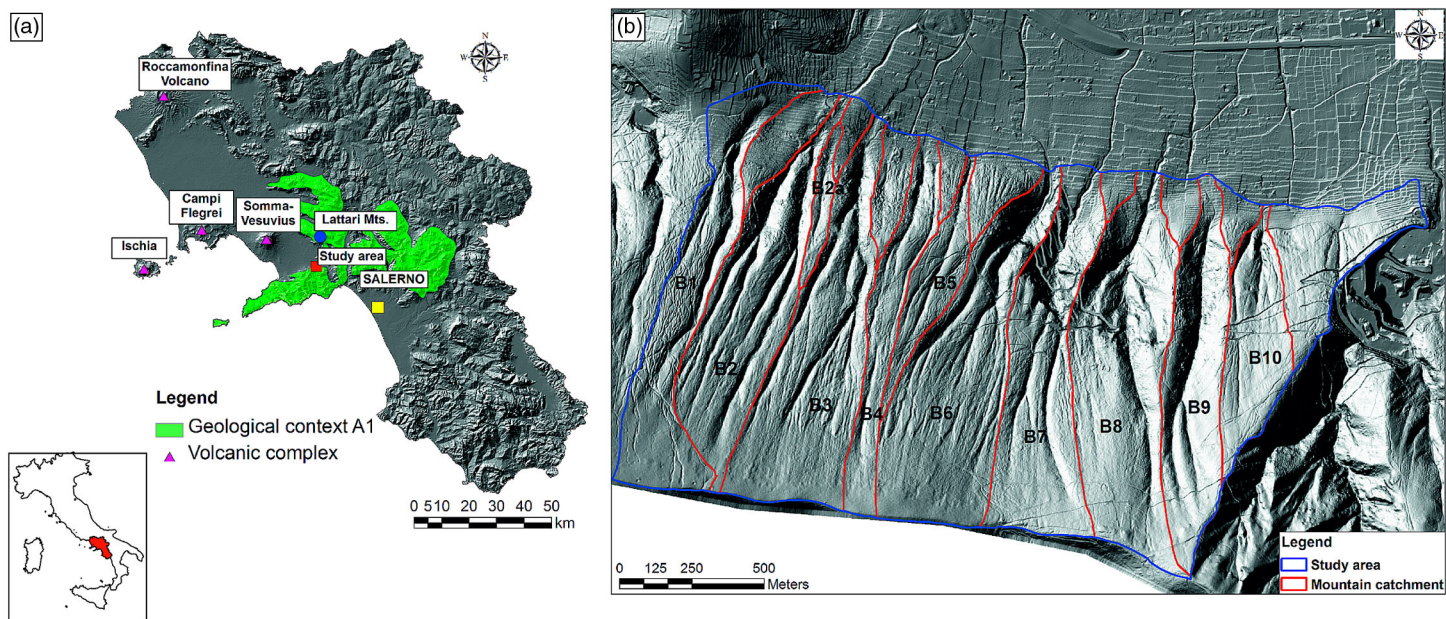

CONTACT Fabio Matano ✉ fabio.matano@cnr.it

Figure 1. (a) DTM (pixel resolution 20 m) of the Campania region (southern Italy) with location of the study area; (b) study area and mountain catchments along the Mount Albino northern slope, superimposed on a DTM derived from 1 m resolution data obtained during a LiDAR survey.

mantle a Mesozoic calcareous bedrock (Bonardi et al., 2009; Di Nocera, Matano, Pescatore, Pinto, & Torre, 2011).

The stratigraphy of pyroclastic cover beds is characterised by the overlapping of different volcanoclastic deposits related to distinct eruptive phases or to different volcanic sources. The resulting stratigraphic complexity is further influenced by sin- and post-depositional erosive processes that often truncate or locally remove the pre-existing pyroclastic strata. Moreover, reworked pyroclastic materials – derived from sheet-wash and mass-wasting processes – can be found at different depths, interbedded with *in situ* pyroclastic materials, while the deepest strata of pyroclastic cover beds can be affected by weathering and cementing.

The morphology of Mount Albino is strongly related to the bedrock geo-structural setting, which is characterised by a stepped longitudinal profile associated with an extensional E–W trending normal fault system (Cascini et al., 2013; Galadini, Meletti, & Vittori, 2000). Figures labelled from A to M are included in the supplementary materials. In particular, it is possible to identify (Fig. A):

- a *sector of alluvial plain with alluvial-debris fans*, with volcanoclastic and alluvial deposits, going down to 30 m a.s.l.;
- a *foot slope to alluvial plain transition sector*, with an average elevation of 200 m a.s.l., which includes the inner portion of debris-alluvial fans, the lower border of open slopes and the outlets of the mountain catchments;
- a *fault slope sector*, rising to about 900 m a.s.l., where the calcareous bedrock is largely covered by debris and volcanoclastic deposits (locally lying on *in situ* cohesionless pumice and ash discontinuous layers), and has evolved by recession processes of the main fault planes. Accordingly, this sector is characterised by a well-developed concave profile in the upper part, a sharp break in slope angles in the middle part (from 380 to 500 m a.s.l.) and a straight profile in the lower steeper part.

Along Mount Albino slope several landforms – related to erosion, transport and deposition processes – can be recognised (Fig. A). The most relevant ones are:

- *morphological hollows* and *zero-order basins* (Dietrich, Reneau, & Wilson, 1987), filled by volcanoclastic and detrital deposits with average thickness exceeding 1–2 m; these landforms are at the head of gullies and are shaped by surface water erosion and colluvial processes;
- *gullies*, characterised by deep channels due to linear erosion processes affecting volcanoclastic-detrital deposits;
- *erosion scarps*, mainly linked to either linear erosion processes along the channels, incising the pyroclastic cover beds (and sometimes also the calcareous

bedrock), or corresponding to buried tectonic elements of the bedrock.

The continuous and progressive reworking of pyroclastic materials from the upper part of the fault slope sector to the alluvial plain sector is generally due to erosion processes along hollows and gullies as well as rainfall-induced slope instabilities along gullies' sides (De Chiara et al., 2015) and at main topographical discontinuities (of either natural or anthropic origin). The latter can turn into debris avalanches (Hungr, Evans, Bovis, & Hutchinson, 2001), as did the March 2005 event (Revellino et al., 2013) that caused three fatalities and the destruction of buildings.

3. The thickness mapping method

The method adopted for the generation of the pyroclastic cover bed thickness map at 1:5000 scale includes the following steps:

- geological and geomorphological analyses;
- *in situ* investigations;
- implementation of a database of the *in situ* measurements and DTM-derived information;
- data processing in a GIS environment;
- map production.

The analysis of topographic attributes (i.e. slope angle, curvature, elevation and aspect), corroborated by air-photo interpretation and geological field survey, allowed the identification of the calcareous rock outcrops and their areal extent, that is, the slope portions where the presence of pyroclastic cover beds is negligible.

The *in situ* investigations were carefully planned taking into account the information gathered from both field surveys and catalogues of records (De Chiara, 2014) dealing with slope instabilities that affected Mount Albino in the past (including both erosion processes and landslides, see Fig. A). The resulting activities – intensive but, at the same time, low-cost – were aimed at collecting data on pyroclastic cover bed thickness and related stratigraphy to be organised and managed in a GIS database. An orthophoto at 1:1000 scale (see Figure with imagery in Main map) and a high-quality DTM of the Mount Albino northern slope, obtained from air-photo surveys and 1 m resolution LiDAR data collected on March 2005, were used as the reference topographic layer in the GIS database.

Data processing was used to estimate pyroclastic cover bed thicknesses in unsampled locations by applying the geostatistical interpolation technique of O.K. The accuracy of the estimates was first checked by comparing the computed thickness values with measured values (collected in a validation database) on the basis of error statistics; then a critical analysis

of O.K. model-related semivariograms and different output maps was carried out in order to identify the most suitable O.K. interpolation to obtain a reliable pyroclastic cover bed thickness map. Finally, the adoption of heuristic criteria supplemented by results of DTM and air-photo interpretation as well as by geomorphological and stratigraphic field information allowed the improvement of geostatistical interpolation results, making the final map a better representation of the actual physical conditions of the study area.

3.1. Data collection

The *in situ* investigations were carried out from November to December 2010; in particular, they included 1197 probings, 60 dynamic penetration tests (DL030), 70 man-made pits, 74 seismic surveys and 18 stratigraphic sections on natural cuts (Figure 2). The global positioning system receiver location of each investigated point was recorded in a GIS environment with a symbol for identifying and visualising the peculiar field test carried out (Figure 2). The steepest portions of the study area, where slope angles exceeded 40°, were not investigated because of limited accessibility and widespread outcropping rock.

Probings were carried out with an iron rod having a diameter of 1.8 cm and a length up to 306 cm. The iron rod, which was inserted into the pyroclastic cover beds by hand or with the aid of a hammer of 0.03 kN in weight, allowed the local measurement of the depth – from the surface – of the contact between the pyroclastic cover beds and the underlying calcareous bedrock (or, in some cases, debris consisting of calcareous blocks in a pyroclastic matrix). Probings were carried out on a 50 m grid (Figure 2). Local values of pyroclastic cover bed thicknesses were calculated as the arithmetical mean of two or three probing measurements recorded within a circular area, centred on a given grid node, with a radius ranging from 1 to 2 m; this working assumption enabled the minimisation of errors related to local factors (such as cobbles and boulders, roots, residual relicts from weathering or colluvium and pumice layers). On landforms (i.e. hollow, zero-order bason and gully) with a high variability of local thickness, the spatial density of probing was increased to 5–10 m between observations (Figure 2).

The DL030 tests consisted of inserting into the ground – with a slide hammer of 0.3 kN in weight and cyclically falling from a height of 20 cm – a probe with a tip section of 10 cm^2 at the end of a system composed of a maximum of 14 iron-rods, each having a circular cross section of 3.57 cm diameter and a length of 1 m. Data collected via these tests agreed with local probing measurements of the total thickness of the pyroclastic cover beds; moreover, they allowed the stratigraphy to be inferred. Further data about stratigraphic profiles were collected from sub-vertical

sections exposed in hand-dug pits (not exceeding 2 m in depth), located near DL030 tests (Figure 2).

Finally, a geophysical survey was carried out with the main aim of gathering information about the shape of the contacts between the different layers forming the cover deposits and the calcareous substratum. The geophysical surveys recorded reflection data from 3 bursts (direct, reverse and intermediate) via the use of 24 geophones spaced 3–5 m apart, placed on the ground surface along a straight line of 60 m. The geophysical data were processed via the INTER-SISM software (Geo & Soft International – www.geoandsoft.com) in order to obtain stratigraphic profiles.

3.2. Database of field measures

Measured and derived data from *in situ* investigations were collected in a database and then managed in a GIS environment.

The probings provided the highest number of input data used in the generation of the pyroclastic cover bed thickness map. Because of the length of the probe, these field tests did not allow the detection of the lithological contact between the pyroclastic cover beds and the calcareous bedrock when the thickness locally exceeded 306 cm. In such cases, probing data were complemented with information gathered from the DL030 tests or the geophysical surveys. With reference to the latter, the seismic profiles were subsampled over a 10-m regularly spaced grid and a total of 300 survey data points were extracted. Comparison with all *in situ* test measurements allowed the identification and the deletion of erroneous data. In total, 1606 thickness measurements were included in the analysis: 1188 probings, 59 dynamic penetration tests (DL030), 41 man-made pits, 73 seismic survey lines reduced to the 300 survey data points and 18 stratigraphic sections on natural cuts. On the steepest portion of the slopes, where *in situ* investigations were unavailable, boundaries of outcropping calcareous rock were also accurately mapped (Fig. B) using slope attributes derived by DTM processing, combined with air-photo interpretation and geological field observations.

An analysis of the *in situ* investigation data (Fig. B) reveals that pyroclastic cover bed thicknesses change rapidly over short distances; therefore, to generate a detailed pyroclastic cover bed thickness map, special attention should be paid to the choice of the most suitable interpolation method.

3.3. Data processing

The interpolation of measured pyroclastic cover bed thickness was carried out using O.K. implemented in the Esri ArcGis 9.3*. In order to choose the most suitable O.K. model (among those listed in Table 1), an
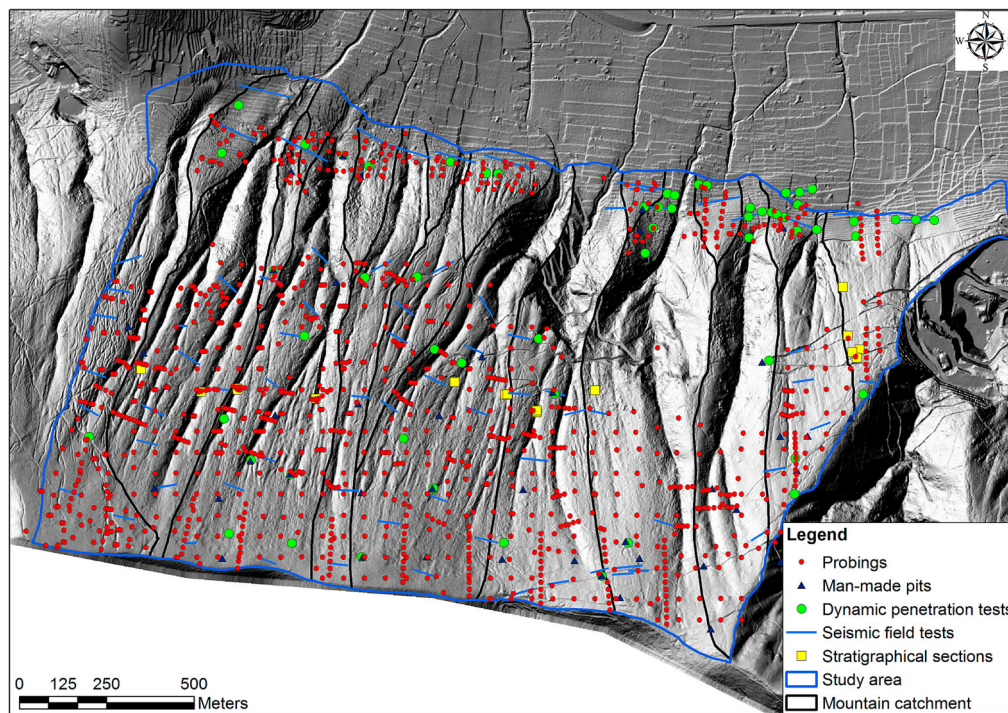
Figure 2. Mount Albino northern slope shaded relief with location of the sites where *in situ* investigations were carried out.

analysis of accuracy was carried out. Errors of difference between the estimated and measured pyroclastic cover bed thickness values were computed by randomly portioning all sample data (Fig. B) into two subsets, namely a training subset including 85% of data and a validation subset including the remaining 15% of data (Fig. C). Using the training subset, different semivariograms were generated; then each data point (i.e. measured value) of the validation subset was compared with the estimated value of the output rasters on the basis of the following statistics (Table 1):

- the mean error (ME), which proves an unbiased estimate if its value is close to 0;
- the root mean square error (RMSE) and RMSE normalised by the observation range (NRMSE), which indicate a better prediction accuracy if their values are as small as possible;
- the coefficient of determination (R^2), ranging between 0 and 1, which quantifies the proportion of variance accounted for in the validation data set.

Since the above statistics did not show significant differences among all analysed O.K. models (Table 1), the choice of the one to be adopted was based on further considerations arising from a critical analysis of (i) the O.K. model-related semivariograms and (ii) the different output maps. Those having the highest ME values (O.K. 3, O.K. 4, O.K. 5, O.K. 6) were rejected.

In order to capture the local spatial data variation, especially over short distances which are the most important for interpolation, a semivariogram with a lag of 25 m was considered. The imposed lag roughly represents the average distance between neighbouring data points. A small lag size (O.K. 2) provides information about the short-distance range of spatial dependence, whose nature is a function of the spatial processes determining variability; whereas a large lag size (O.K. 7, O.K. 8) implies a loss of information about the shape of the semivariogram for short distances and less information about the shape over all (in this case the minimum and maximum predicted value differs from the measured ones). In order to avoid bias in a particular direction and to capture the short-distance dissimilarity, the predicted value at an unmeasured location was derived by the interpolation of a maximum of five data points enclosed in a circle of a fixed radius equal to the range of the semivariogram (i.e. representing the maximum distance within which there is a spatial correlation) that in turn was subdivided into four sectors from which an equal number of points were selected. The models with a variable radius (O.K. 9) provided unreliable predicted values at unmeasured locations where validation data points are also lacking.

As for the directional influence affecting pyroclastic cover bed thickness along the slope and mainly related to physical processes (i.e. wind, runoff and erosion), different anisotropic semivariograms were analysed. Unlike the isotropic models for which the best is O.K. 1, the most reliable anisotropic model was derived by decreasing the lag size to 10 m (O.K. 13) with a consequent reduction of the major and minor axes of the elliptical range distribution which takes into account the local spatial data variation along a specific direction

Table 1. Accuracy analysis of pyroclastic cover bed thickness associated with different geostatistical interpolation methods.

Name	Model	Lag	Range	Neighbors	Min (*) (m)	Max (*) (m)	ME (m)	RMSE (m)	NRMSE (–)	R^2 (–)	Number of validation points
O. K. 1	Spherical and isotropic	Size: 25 m Number: 12	45.5 m	Included: 5 Type: circle with radius $r = 45$ m	0	14.5	0.07	1.65	0.12	0.22	230/241
O. K. 2	Spherical and isotropic	Size: 5 m Number: 11	30 m	Included: 5 Type: circle with radius $r = 30$ m	0	14.5	−0.01	1.63	0.12	0.26	205/241
O. K. 3	Circular and isotropic	Size: 25 m Number: 12	45.5 m	Included: 5 Type: circle with radius $r = 45$ m	0	14.5	0.08	1.65	0.12	0.22	230/241
O. K. 4	Exponential and isotropic	Size: 25 m Number: 12	45.5 m	Included: 5 Type: circle with radius $r = 45$ m	0	14.5	0.08	1.66	0.12	0.22	230/241
O. K. 5	Gaussian and isotropic	Size: 25 m Number: 12	45.5 m	Included: 5 Type: circle with radius $r = 45$ m	0	14.5	0.08	1.65	0.12	0.22	230/241
O. K. 6	Stable and isotropic	Size: 25 m Number: 12	45.5 m	Included: 5 Type: circle with radius $r = 45$ m	0	14.5	0.08	1.65	0.12	0.22	230/241
O. K. 7	Spherical and isotropic	Size: 200 m Number: 10	1985 m	Included: 5 Type: circle with radius $r = 1985$ m	0.4	7.6	0.0	1.56	0.11	0.25	241/241
O. K. 8	Spherical and isotropic	Size: 100 m Number: 10	992 m	Included: 5 Type: circle with radius $r = 992$ m	0.4	7.6	0.0	1.56	0.11	0.25	241/241
O. K. 9	Spherical and isotropic	Size: 25 m Number: 12	45.5 m	Included: 5 Type: circle with variable radius	0.2	8.9	−0.02	1.63	0.12	0.21	241/241
O. K. 10	Spherical and anisotropic	Size: 25 m Number: 12	Major: 296 m Minor: 63 m Direction: 345°	Included: 5 Type: ellipse with radius $R = 296$ m and $r = 63$ m	0	11.3	0.0	1.63	0.12	0.20	241/241
O. K. 11	Spherical and anisotropic	Size: 5 m Number: 11	Major: 55 m Minor: 9 m Direction: 273°	Included: 5 Type: ellipse with variable radius	0	12.4	0.03	1.63	0.12	0.24	241/241
O. K. 12	Spherical and anisotropic	Size: 20 m Number: 10	Major: 199 m Minor: 62 m Direction: 341°	Included: 5 Type: ellipse with radius $R = 199$ m and $r = 62$ m	0	11.3	−0.01	1.59	0.11	0.23	241/241
O. K. 13	Spherical and anisotropic	Size: 10 m Number: 10	Major: 99 m Minor: 16 m Direction: 92°	Included: 5 Type: ellipse with radius $R = 99$ m and $r = 16$ m	0	14.5	−0.06	1.58	0.11	0.30	229/241
O. K. 14	Spherical and anisotropic	Size: 15 m Number: 10	Major: 149 m Minor: 24 m Direction: 91°	Included: 5 Type: ellipse with radius $R = 149$ m and $r = 24$ m	0	12	0.02	1.57	0.11	0.28	241/241
O.K. 15	Spherical and anisotropic	Size: 5 m Number: 11	Major: 55 m Minor: 9 m Direction: 273°	Included: 5 Type: ellipse with radius $R = 55$ m and $r = 9$ m	0	14.5	−0.15	1.71	0.12	0.31	171/241

Note: Asterisked columns refer to minimum (Min) and maximum (Max) values of estimated thicknesses.

(Table 1). Visual comparison of the output maps of O. K. 1 and O.K. 13 (Fig. C) reveals that both models produce strong patterns (circular in the isotropic model and elliptical in the anisotropic one) that require further work to bring the map more in line with reality. On the other hand, the use of the anisotropic model can lead to a considerable loss of spatial information, especially in the fault slope sector where predicted pyroclastic cover bed thickness values are largely lacking. On the other hand, the isotropic model allows the local spatial variability of pyroclastic cover bed thickness to be more evident.

Therefore, among the investigated models, O.K. with a spherical and isotropic semivariogram (O.K. 1), a nugget value of 1.36, a maximum range of 45.5 m and a partial sill of 0.18 was considered to be the most suitable for geostatistical interpolation analysis purposes.

3.4. Heuristic post-processing

The pyroclastic cover bed thickness map obtained from the adoption of the O.K. 1 geostatistical interpolation method (Fig. D) has some shortcomings; in particular:

(a) the map is incomplete in the peripheral and steep sectors of the study area where measurements are lacking;

(b) there is a local bias in thickness values provided by O.K. with reference to measured values;

(c) there is a local inconsistency between the distribution of kriged values and the recognised morphological elements.

To compile the final map of pyroclastic cover bed thickness, a heuristic procedure was adopted. This consisted of integrating and amending the kriging results on the basis of qualitative information, such as that gathered from geological field surveys along with air-photos and DTM-derived geomorphological interpretations. Figure E shows some sample areas for which the improvements deriving from the adoption of post-processing procedures are explained below.

Before addressing the shortcomings, the kriging output raster was set to a pixel size of 5 m according to the final map scale which was fixed at 1:5000. The raster map was converted to a polygon shapefile useful for post-processing analysis purposes (Fig. F).

The pyroclastic cover bed thickness map was completed for the whole study area by locally assigning thickness values to the slope sectors without kriged data. On the steepest slopes, the boundaries of the outcropping calcareous rock were accurately mapped using an incline threshold value of 45° derived from DTM analysis, combined with air-photo interpretation and geological field observations (Fig. G). In the peripheral sectors of study area, the map was completed by extrapolating the available field data following the slope morphology and elevation ranges (Fig. H).

For slope sectors with kriged data, some manual adjustments to polygons were made after:

(a) local checking of measured vs. kriged thickness values of the pyroclastic cover beds;

(b) checking of the consistency between the kriged thickness values and morphological elements;

(c) identification of artefacts due to the kriging process.

Results of the first check highlighted two possible kinds of local discrepancies, depending on measured thickness values which can be higher or lower than corresponding kriged ones. In the first case, the map was directly amended by imposing the coincidence of measured and kriged thickness values. In the second case, correction was not required when measured values are clearly affected by local conditioning factors, such as the presence of isolated boulders in the pyroclastic cover beds. In other circumstances, the map was adjusted taking into account either the geomorphological aspects locally characterising the slope

portion at hand or the information associated to nearby probing measurements.

As for the second check, the kriged values were modified with reference to local conditions in the areas where morphological elements strongly control the spatial variability of pyroclastic cover bed thickness. In particular, in concave (e.g. hollows, zero-order basins, gullies) and convex (e.g. ridges) sectors of the slope, thickness values tend to be similar along the axis direction of morphological elements (i.e. along maximum slope angles). Accordingly, in the post-processing phase of the work, the kriged thickness values were adjusted depending on the local concavity (Fig. I and J) or convexity (Fig. J). On the other hand, thickness values along calcareous scarps tend to be similar orthogonal to maximum slope angles (Fig. J). In the detachment area of the debris avalanche that occurred on March 2005, the thickness values were reduced in the depletion sector on the basis of field observations (Fig. K).

Thirdly, the observed circular trends in kriged pyroclastic cover bed thickness values – which are unrelated to existing landforms (Fig. A) – are a consequence of the maximum threshold (45 m) of the nearest observation point, beyond which an interpolated value is not computed. In these cases, they were manually adjusted on the basis of local geomorphological conditions (Fig. L).

The heuristic post-processing of geostatistical interpolation results involved about 20% of the study area and largely concentrated on the foot slope to alluvial plain transition sector (Fig. M); the resulting pyroclastic cover bed thickness map has about 5,300 polygons. Twenty-two per cent of these were characterised by an area with an extent of less than 5 m^2. In order to delete unnecessary details about the distribution of thickness values obtained by kriging, each isolated polygon smaller than 5 m^2 was aggregated to the largest neighbouring polygon with close thickness values.

4. The pyroclastic soil thickness map

The pyroclastic cover bed thickness distribution over Mount Albino, shown on the main map printed at 1:5000 scale, was compiled with 16 depth classes. These classes were chosen to best represent the spatial variability of pyroclastic cover bed thickness over the study area. The first class relates to outcropping calcareous rock; the following 10 and 4 classes correspond to classes of pyroclastic cover bed thicknesses of 0.5 and 1 m, respectively; the last one going to the maximum estimated value.

Spatial variability is strongly controlled by the buried morphology of the calcareous bedrock as well as the different geomorphological processes taking place along the slope. Where slope angles are lowest and

the morphology is more conservative and less susceptible to erosion (e.g. ridges) most of the maximum thickness of the air-fall pyroclastic deposits is preserved. In contrast, bare areas correspond to steep morpho-structural slopes and to channels eroded in bedrock. In detail, the thickness values range from a minimum of 2 m to a maximum of 4.5 m in the western part of the study area (mountain catchment B1), as well as along the ridges and the upper sections of the slope where morphological concavities or karstic depressions filled by pyroclastic soil can be recognised. In the middle part of the fault slope sector thickness values do not generally exceed 1.5–2 m, even though locally pyroclastic cover beds that are 3.5 m thick can be found. In the steepest areas, thickness values are generally lower than 0.1 m, especially in the lateral sectors of gullies, while, in the transition sector of the slope, they reach the highest values (locally greater than 5 m) due to reworking and deposition processes caused by both landslide events and erosion processes.

5. Conclusions

This paper describes a method for estimating and mapping – at a scale of 1:5000 – the thickness of pyroclastic cover beds resting on calcareous bedrock. The method requires the availability of field data (i) achieved via low-cost and easy-to-use instruments (e.g. iron-rod probings), (ii) later managed in a GIS environment through a well-adopted geostatistical interpolation technique (i.e. O.K.) and (iii) finally integrated or amended using heuristic criteria that benefit from the availability of field survey information along with airphotos and a high-quality DTM.

The resulting thickness maps are important for analysing and zoning the susceptibility of slopes to instabilities (including erosion processes and landslides) which involve pyroclastic cover beds. Detailed knowledge of the spatial variability of pyroclastic cover bed thickness also enables the use of advanced numerical models for hazard analyses aimed at simulating both triggering and propagation stages of slope instabilities.

The next stage of the research will focus on the development of an integrated analysis of both *in situ* stratigraphic data and laboratory test results for a detailed estimation and mapping of the stratigraphic settings of pyroclastic cover beds.

Software

The management, archiving, processing and geostatistical analysis of data derived from *in situ* investigation was carried out using Esri ArcGIS 9.3.

The data acquired with seismic refraction profiles were processed using the commercial software INTERSISM (Geo & Soft International – www.geoandsoft.com).

The main map was drawn with COREL DRAW X7.

ORCID

Fabio Matano http://orcid.org/0000-0001-7021-9364
Giovanna De Chiara http://orcid.org/0000-0002-8931-4617
Settimio Ferlisi http://orcid.org/0000-0003-0500-3369
Leonardo Cascini http://orcid.org/0000-0003-2807-6990

References

Amundson, R., Heimsath, A., Owen, J., Yoo, K., & Dietrich, W. E. (2015). Hillslope soils and vegetation. *Geomorphology*, *234*, 122–132.

Bonardi, G., Ciarcia, S., Di Nocera, S., Matano, F., Sgrosso, I., & Torre, M. (2009). Carta delle principali unità cinematiche dell'Appennino meridionale – Nota illustrativa. *Bollettino della Società Geologica Italiana*, *128*, 47–60.

Cascini, L., Di Nocera, S., Calvello, M., Cuomo, S., Ferlisi, S., & Matano, F. (2013). Hyperconcentrated flow susceptibility analysis and zoning at medium scale: methodological approach and case study. In C. Margottini, P. Canuti, & K. Sassa (Eds.), *Landslide science and practice* (Vol. 1: Landslide Inventory and Susceptibility and Hazard Zoning, pp. 395–402). Cham: Springer International.

Cascini, L., Ferlisi, S., & Vitolo, E. (2008). Individual and societal risk owing to landslides in the Campania region (southern Italy). *Georisk*, *2*(3), 125–140.

Catani, F., Segoni, S., & Falorni, G. (2010). An empirical geomorphology based approach to the spatial prediction of soil thickness at catchment scale. *Water Resources Research*, *46*(5), 1–15.

De Chiara, G. (2014). *Quantifying the risk to life posed by hyperconcentrated flows* (PhD Thesis). University of Salerno, Italy.

De Chiara, G., Ferlisi, S., Cascini, L., & Matano, F. (2015, September 24–25). Rainfall-induced slope instabilities in pyroclastic soils: The case study of Mount Albino (Campania region, southern Italy). In T. Rotonda, M. Cecconi, F. Silvestri, & P. Tommasi (Eds.), *Volcanic rocks and soils* Proceedings of the International Workshop on Volcanic Rocks and Soils – Lacco Ameno, Ischia Island, Italy, pp. 327–333. London: CRC Press, Taylor & Francis Group.

De Vita, P., Napolitano, E., Godt, J. W., & Baum, R. L. (2012). Deterministic estimation of hydrological thresholds for shallow landslide initiation and slope stability models: Case study from the Somma-Vesuvius area of Southern Italy. *Landslides*, 10, 713–728.

Di Nocera, S., Matano, F., Pescatore, T., Pinto, F., & Torre, M. (2011). Geological characteristics of the external sector of the Campania-Lucania Apennines in the CARG maps. *Rendiconti Online Società Geologica Italiana*, 12(Suppl.), 39–43.

Dietrich, W. E., Reiss, R., Hsu, M. L., & Montgomery, D. R. (1995). A process based model for colluvial soil depth and shallow landsliding using digital elevation data. *Hydrological Processes*, 9, 383–400.

Dietrich, W. E., Reneau, S. L., & Wilson, C. J. (1987, August 3–7). Overview: Zero order basins and problems of drainage density, sediment transport and hillslope morphology. In R. L. Beschta, T. Bilnn, G. E. Grant, G. Ice, & F. J. Swanson (Eds.), *Erosion and sedimentation in the Pacific Rim*, Proceedings of the Corvallis Symposium, held at Oregon State University, Corvallis, OR. International Association of Hydrological Sciences, 165, 27–37. Wallingford: IAHS Press.

Galadini, F., Meletti, C., & Vittori, E. (2000). Stato delle conoscenze sulle faglie attive in Italia: elementi geologici di superficie. Risultati del progetto 5.1.2 "Inventario delle faglie attive e dei terremoti ad esse associabili". In F. Galadini, C. Meletti, & A. Rebez (Eds.), *Le ricerche del GNDT nel campo della pericolosità sismica (1996–1999)* (pp. 107–136). Roma: CNR-Gruppo Nazionale per la Difesa dai Terremoti.

Hungr, O., Evans, S. G., Bovis, M. J., & Hutchinson, J. N. (2001). A review of the classification of landslides of the flow type. *Environmental & Engineering Geoscience*, 7 (3), 221–238.

Kuriakose, S. L., Devkota, S., Rossiter, D. G., & Jetten, V. G. (2009). Prediction of soil depth using environmental variables in an anthropogenic landscape, a case study in the Western Ghats of Kerala, India. *Catena*, 79, 27–38.

Lucà, F., Buttafuoco, G., Robustelli, G., & Malafronte, A. (2014). Spatial modelling and uncertainty assessment of pyroclastic cover thickness in the Sorrento Peninsula. *Environmental Earth Sciences*, 72(9), 3353–3367.

Revellino, P., Guerriero, L., Gerardo, G., Hungr, O., Fiorillo, F., Esposito, L., & Guadagno, F. M. (2013). Initiation and propagation of the 2005 debris avalanche at Nocera inferiore (Southern Italy). *Italian Journal of Geosciences*, 132, 366–379.

Rolandi, G., Paone, A., Di Lascio, M., & Stefani, G. (2007). The 79 AD eruption of Somma: The relationship between the date of the eruption and the southeast tephra dispersion. *Journal of Volcanology and Geothermal Research*, 169, 87–98.

Segoni, S., Rossi, G., & Catani, F. (2012). Improving basin scale shallow landslide modelling using reliable soil thickness maps. *Natural Hazards*, 61, 85–101.

Taylor, R., & Eggleton, A. (2001). *Regolith geology and geomorphology*. Chichester: John Wiley & Sons.

Uchida, T., Tamura, K., & Akiyama, K. (2011). The role of grid cell size, flow routing algorithm and spatial variability of soil depth on shallow landslide prediction. *Italian Journal of Engineering Geology and Environment*, 11, 149–157.